Charge-Mediated Cation Deposition on Metallic Surfaces

Journal:	*Journal of Materials Chemistry A*
Manuscript ID	TA-ART-01-2019-000987.R1
Article Type:	Paper
Date Submitted by the Author:	05-Mar-2019
Complete List of Authors:	Longo, Roberto; Texas A&M University System, Chemical Engineering Camacho-Forero, Luis; Texas A&M University, Chemical Engineering Balbuena, Perla; Texas AandM University, Chemical Engineering

SCHOLARONE™
Manuscripts

Charge-Mediated Cation Deposition on Metallic Surfaces

Roberto C. Longo*, Luis E. Camacho-Forero and Perla B. Balbuena*

Department of Chemical Engineering, Texas A&M University, College Station,

Texas 77843, United States

*E-mails: roberto.longo@tamu.edu, balbuena@tamu.edu

Abstract

This work reveals the general mechanisms of Li^+ cation partial reduction and further deposition under specific electrolyte conditions, and in the proximity of an electrified metal surface. The factors affecting the ion complexation and transport and resultant adsorbed structures are identified for various external electric fields and for several applied voltages. Using *ab initio* methods, we investigate the relation between solvent-salt structures and dynamics, cation reductive stability, and the existing electric field between electrodes, or under the applied potential if the system is designed as an electrochemical cell. In absence of an applied field, it is found that not only cation but also non-solvated salt deposition on a metallic surface is an endothermic process. However, localized surface polarization orbitals created by an external electric field affect both the thermodynamics and kinetics of the adsorption, leading to a drastic change on the energetic profile; *ab initio* Molecular Dynamics simulations describe in detail the underlying mechanisms. Externally applied bias to an electrochemical cell also changes the deposition dynamics: By examining various solvent/salt combinations, we unravel the cation deposition mechanisms at both low and moderately high voltages, determining the relative time scale of each separate process. Different polyhedra formed

by the metal cation and its surrounding oxygen atoms appear to be the key indicator driving deposition dynamics at different voltages. Our findings disclose the importance of selecting appropriate voltage windows for stable and uniform growth of metal anode layers, showing the mechanisms leading to impurity formation and non-uniform cation deposition, as well as the role of charged interfacial phenomena in designing stable electrode-electrolyte interfaces.

Introduction

During the last two decades, intensive research efforts have been focused on the improvement of the capacity, cyclability, safety and faster charging times of current Li-ion batteries (LIB)[1,2]. Batteries are now ubiquitous in today's life[3,4], not only because they are the main power source for rechargeable electronic devices and electric vehicles[5,6], but also because there is finally a consensus in both the scientific community and the industry in the sense that the future is going to be "electric", that is, heavy transport and the electric grid will also rely on rechargeable batteries to store energy and secure their daily operations[7,8].

The electrolyte-electrode interface is the key component determining the performance of LIB[9]. The molecular structure, ion (de)-solvation and transport into the electrodes for oxidation-reduction are ultimately responsible for the structural deterioration as well as capacity fading and poor cycling performance, all of which are well-known problems preventing the expanse of present battery technologies to the aforementioned massive energy storage applications[10]. Current negative electrodes are basically graphite-based materials[11], due to the intrinsic instability in contact with liquid electrolytes of higher capacity anode materials such as silicon or lithium metal itself[12]. Alternative battery chemistries with superior properties like Li-S or Li-air are actively considering the use of lithium metal as the anode, yet issues such as high reactivity, non-reversible

plating/stripping, dendrite formation or "mossy" growth still remain[13]. However, recent progress on solid ionic conductors have opened the door to the use of all-solid batteries, rising enormous expectations in terms of improved safety, electrochemical, mechanical and thermal stability[14]. In addition, recent improvements in liquid electrolytes make further expectations on a successful control of the Li metal anode/electrolyte interface.[15-18]. It is within this context where the use of Li metal as the negative electrode achieves considerable importance, as it represents the ideal material in terms of energy density, source of conducting ions and structural interface with Li-containing solid ionic conductors[19] or well-designed liquid electrolytes[16]

A key parameter for the Li-metal-battery performance is the electrochemical stability of a solid or liquid electrolyte in contact with the metal anode. This has become the focus of many experimental and theoretical studies[20-23]. A proper treatment of the absolute reference for oxidation/reduction potentials, accounting for the screening of charged systems as well as interfacial chemical reactions, ion diffusion pathways and transition states constitute a major challenge for theoretical studies[24]. However, little effort has been dedicated to explore the initial deposition of the lithium metal itself and, more specifically, to analyze the chemical reactions, electrochemically charged interfaces and the reaction pathways leading from a solvated, Li-containing salt to Li ion deposition on a metallic surface. Indeed, the transition from a fully charged and high coordination form of the metal cation to a partially reduced, non-coordinated form after deposition is largely unclear. The proximity of an electrified substrate necessarily impacts the metal coordination and the salt-solvent dynamics. Moreover, the time scale of salt-solvent composite reorganization and electron transfer during cation deposition will be inevitably affected by the magnitude of the external potential. Electron transfer for cation reduction can occur at significant overpotentials, in order to overcome the salt-solvent high coordination or by formation of new cation-solvent composites, whereas close to a polarized metallic substrate electron transfer is necessarily facilitated by reduced cation

coordination, assisted by salt-solvent combined dynamics[12,24,25]. Needless to say, an explicit description of such charged electrochemical cation deposition process by means of first-principles methods becomes clearly necessary.

In the present work, our aim is to study the deposition of Li^+ ions on a model metal surface (Cu001) (similar to those used for Li electrodeposition studies[26]) from several combinations of salts (namely LiFSI, LiTFSI and $LiNO_3$) and solvents (DME and DOL), in pursuit of understanding the effect of having charged interfaces and, therefore, establishing a voltage dependence of the Li deposition process from different constituents. As we are interested in accounting for the salt-solvent interaction explicitly and its effect on cation deposition, no implicit solvent models were used. Instead, the explicit atomistic structure of the molecules involved on Li deposition was considered, and the structural evolution was analyzed by means of *ab initio* molecular dynamics (AIMD), kinetic calculations and charged electrochemical interfaces. This work is divided in two parts. First, we study the deposition of Li ions under the effect of an external electric field, when the system is embedded between two electrodes, that is, like a slab placed in a capacitor. The second part shows the effect of the external potential on the molecular evolution and Li deposition when the system is configured like an electrochemical cell, *i.e.*, the slab surface is placed between an electrode and the vacuum. Our results shed light not only on the ion deposition process but also on the effect of having a charged surface on the structural evolution of the salt-solvent combined system, showing clearly the formation of intermediate composites as the necessary key leading ultimately to Li deposition.

Methodology

The calculations performed in this work include the optimization of neutral Li molecular organic salts, namely lithium bis(fluorosulfonyl)imide ($LiF_2NO_4S_2$, LiFSI), lithium

bis(trifluoromethane)sulfonimide ($LiC_2F_6NO_4S_2$, LiTFSI) and lithium nitrate ($LiNO_3$). Also, two molecular solvents were used: 1,2-dimethoxyethane ($C_4H_{10}O_2$, DME) and 1,3-dioxolane ($C_3H_6O_2$, DOL). The optimized molecular structures were taken from our previous publications[27,28], and combined into the same system as described below. Our basic premise is that the stability of the organic salt is dictated by the electrochemical stability of the Li^+-containing molecule and its (partially) reduced form after dissociation and adsorption, *i.e.*, we limit the analysis only to an electron transfer process [29], without further considerations about thermal activation of coexistence between different charged species, as the main goal of this work is to investigate the effect of the external electric field and/or applied potential on cation deposition. To that extent, for one of the systems (DME-solvated LiTFSI) we have also considered two coordinated configurations (the so-called low and high density solvent), in order to investigate the correlation between the atomistic solvation structure and the speed of the cation adsorption and reduction mechanism. No assumptions have been made about the relative time scales of the intrinsic electron transfer, but the use of AIMD simulations allows us to obtain approximate deposition times, instead of performing a full analysis of the free energy landscape, kinetic energy barriers and local minima, which would be much more computationally demanding.

Quantum Chemistry Calculations. The calculations of the optimized geometries, relative energies and orbital occupancies were performed using density-functional theory (DFT) within the generalized gradient approximation (GGA), as implemented in both Quantum Espresso (QE) [30,31] and the Vienna *ab initio* simulation package (VASP) [32,33]. The electron-ion interaction was described within the projector-augmented wave (PAW) [34,35] scheme (VASP) or by means of ultrasoft pseudopotentials (QE) [36]. The electronic wave functions were expanded into plane waves up to a kinetic energy of 400 eV. The Cu(001) slab was modeled by a 4x4x2 supercell, which comprises 4 layers of 32 atoms per layer, plus solvent and salt molecules and a vacuum region of approximately 30 Å,

large enough to avoid interactions between the system and its replica images. The cell length is 45 Å. In each case, one cation-containing salt molecule and six or eight solvent molecules (depending on the low or high density solvent structure considered) were added to the system, for an overall number of atoms of approximately 200. All the atoms and degrees of freedom, except the bottom Cu layer, were allowed to relax *via* a conjugate gradient technique until the forces on the atoms were below 1 meV/Å. The Brillouin zone integration was performed using a 4x4x1 mesh within the Monkhorst-Pack scheme[37], and the PBE functional was used to describe the electron exchange and correlation energies within the GGA[38]. In addition to PBE, Grimme's empirical dispersion correction with the DFT-D3 parameterization was used to account for weak van der Waals molecular interactions [39,40], because it was found that such combination of functionals produces excellent results in describing molecular solvation structures and dynamic mechanisms[41]. The kinetic energy barriers for molecular dissociation and cation deposition were obtained with the climbing image nudged elastic band (CI-NEB) method[42-44], using a string of geometric configurations to describe the reaction pathways of salt-solvent interactions and further cation deposition on the Cu(001) surface. A spring interaction between every configuration ensured continuity of the reaction pathway.

ESM Calculations. For the solvated salt molecules, the alignment of the cation state with respect to the Cu substrate Fermi energy at different distances was obtained using the effective screening medium (ESM) method [45-47], as implemented in the QE package (henceforth ESM QE calculations). The basic idea behind the method is solving the Poisson's equation under open boundary conditions (OBC, thus setting especial conditions for the dielectric permittivity depending on the electrode environment) across all the space along the direction perpendicular to the slab surface, separately from the standard DFT Kohn-Sham equation defined for the equivalent finite cell with periodic boundary conditions (PBC). In the adiabatic limit, the ground state electronic density determines uniquely the electronic properties of the system, which is then characterized

by the common Fermi energy. We then use such common Fermi energy to account for electron transfer between the cation and the solvent or (if any) the substrate and the cation after adsorption. The substrate+molecular species systems were modeled in the same manner as previously described, but the distance between the upper layer of the substrate and the fictitious electrode was set to 50 Å, in order to provide enough free space between electrodes for the molecular species. Two settings can be investigated within the ESM method: i) the system is placed between two electrodes (that is, two regions with $\varepsilon=\infty$ limiting the OBC space). Such configuration would be equivalent to locate the slab and the molecular species between the two layers of a capacitor, and allows the study of the effect on an external electric field, applied between the two layers of the capacitor. In the second setting: ii) the system is placed between an electrode (upper part) and the vacuum (bottom part), which corresponds to a region with $\varepsilon=1$ limiting the lower part of the OBC. This setting equates to an electrochemical cell, and is used to investigate the effect of an externally applied bias on cation deposition. To determine the common Fermi level under any specific bias, the position of the cation was kept fixed and the rest of the system was relaxed. In all other simulations, all the atomic positions were allowed to relax except the bottom layer of the Cu slab.

Ab Initio Molecular Dynamics Simulations. AIMD simulations were conducted for the cation-containing salts, solvent molecules and the Cu substrate at the PBE+Grimme level, as implemented in both VASP and QE (here including the two ESM QE settings described above) [30,31,33,48]. For all AIMD simulations, the energy grid cutoff was set to the same value as for the corresponding non-dynamic, relaxation calculations, but the total energy was sampled in a *k*-point mesh of 2x2x1. Using a sample time of 1 fs, simulations up to 10 ps were performed (depending on each specific ESM QE case and molecular system) within the canonical NVT ensemble using the velocity Verlet algorithm at 300 K with the Nosé-Hoover thermostat. The simulation box comprises a vacuum region of 50 Å, large enough to ensure convergence of the ESM QE effective region. In

order to accelerate the AIMD simulations and be able to obtain useful information about the effect of the external, fixed potential on cation deposition, we adopted a combined strategy using both VASP and ESM QE packages. The algorithm is described in detail in the Supporting Information, and it basically relies on the equivalence between the applied bias and its effect on the Fermi level and the resulting charge state of the system. All the results discussed in this work correspond to the final AIMD configurations using ESM QE.   Other applications of the ESM methodology to electrode/electrolyte interfaces have been reported recently.[49,50]

Results and Discussion

Electric field-induced electronic and kinetic effects on Li deposition on Cu(001).

a) *Kinetic and electronic effects of cation deposition*. Both the structure of the LiFSI molecule and the DME solvent molecules coordinating the Li cation are to a large extent predetermined by the corresponding preferred configurations of their respective bulk solutions, as well as the dynamics of the electron transfer from the cation and the solvent relaxation. We begin our study by examining such equilibrium configurations: LiFSI solvated by DME in the presence of the metallic Cu(001) surface.

The results of our calculations show (Figure 1) that, at the relatively low concentrations considered in this work (note that such low molecular concentration is a necessary requirement in order to unravel the effects of the external electric field, the ultimate goal of this study), the structure of the DME-solvated LiFSI scarcely differs from the ideal, almost linear configuration. In the most stable configuration, as shown in Figure 1a, Li is coordinated by three oxygen atoms (two of the anion and one of DME), in agreement with similar studies[24]. The corresponding bond lengths and atomic charges are summarized in Table S1.
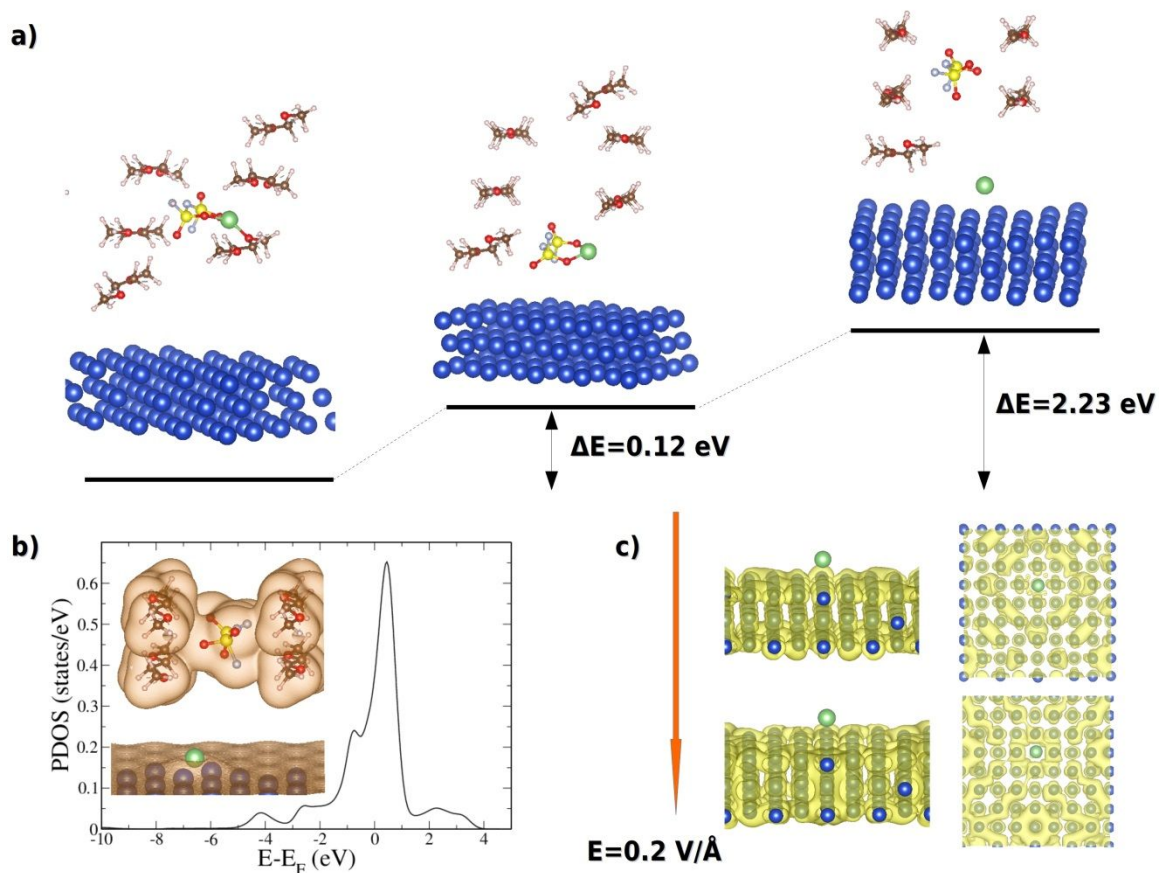
Figure 1. a) Energy profile of Li deposition on Cu(001) from DME-solvated LiFSI in absence of an external field. ΔE values are energies relative to the initial configuration shown at the left. It takes 0.12 eV to break the LiO bond of the salt cation with DME, and 2.23 V to deposit the naked cation on the surface. b) At the condition of naked cation deposition, PDOS of the partially reduced Li $1s$ orbital, after adsorption on Cu(001). Far from the surface, the Li $1s$ orbital is located in the unoccupied region, at the right of the Fermi level. Note that at the surface, the Li $1s$ peak shifts toward the Fermi level, indicating partial reduction. The inset shows the charge density distribution. c) Polarization orbitals created on the Li/Cu(001) system by an external electric field (E_f) of 0.2 V/Å. The polarized orbitals are shown in yellow. Substrate and molecules are embedded between two electrodes (not shown), within the ESM QE framework. Color code: Cu, blue; Li, green, O, red; C, brown, H, white; S, yellow; F, light purple; and N, light blue balls.

Interestingly, most of the electron transfer from the Li⁺ cation goes to the FSI⁻ anion, thus imposing a practical limit to the solvent concentration around each (LiFSI)⁰ molecule.

Within this configuration, the electronic density is delocalized over the FSI$^-$ unit, whereas the vacant orbital is largely localized on the Li cation, as expected [27,28]. The triple oxygen coordination around the Li cation constitutes a thermodynamically strong stable state. The first consequence is that non-solvated, LiFSI molecular deposition on the Cu(001) surface is an endothermic process, with a small reaction energy of 0.12 eV (Figure 1a, middle), but the adsorption of the Li$^+$ cation costs as much as 2.23 eV (Figure 1a, right). After deposition, Li$^+$ gets only partially reduced (see the 1s PDOS in Figure 1b), due to the noble metal-character of Cu. Therefore, cation reduction at the Cu(001) surface is an insufficient condition for Li growth. The question now is, how does an external electric field modify the correlation between the Li 1s vacant orbital and the corresponding adsorption energy? As described in the Methodology section, the ESM QE method replaces standard PBC by OBC. Then, in practice, the system behaves like a slab in a capacitor, that is, embedded between two electrodes with $\varepsilon_r = \infty$. At this point, it is necessary to say that the electrolyte-electrode structure is also crucial to improving electric double layer capacitors, as it is key to understand differential capacitance as well as storage capacity [20]. We will show later the results of such a differential capacitance analysis. The external electric field applied between the two electrodes is represented as a dipole sheet located at the center of the supercell, with opposite charge to that of the electric field. Therefore, the slab polarizes in response. Surface polarization greatly affects Li$^+$ adsorption energies. Moreover, although weakly, the LiFSI-DME molecular complex is also be affected by the applied field. Then, one should expect that both the kinetics and energetics of DME-solvated LiFSI dissociation and further Li$^+$ deposition are going to be modified by the effect of an external electric field applied between the two electrodes.

Indeed, the main effect of such electric field is the polarization of the Cu(001) surface. This results in the formation of new polarization orbitals (see Figure 1c) in both the Cu surface atoms and the hypothetical adsorbed species. This include for instance,

polarization 4*p* and 2*p* orbitals for Cu atoms and the Li$^+$ ion, respectively. These new, (practically) vacant polarization orbitals obviously increase the cation-metal Coulomb attraction, resulting in strengthened adsorption energies.

For the above described DME-solvated LiFSI molecule, in order to achieve the desired cation deposition, a triple Li-O bond needs to be broken. Our calculations show that the most likely mechanism is a two-step process: i) first, desolvation of the LiFSI molecule, that is, the rupture of the stretched cation-oxygen bond, and ii) dissociation of the LiFSI salt molecule. As said before, this is basically a kinetics driven reaction, and we do not expect the electric field playing a determinant role on the mechanism. The obtained results, shown in Figure 2, confirm all these assumptions. The complete list of reaction energies and activation barriers are included in Table S2 (Supporting Information).
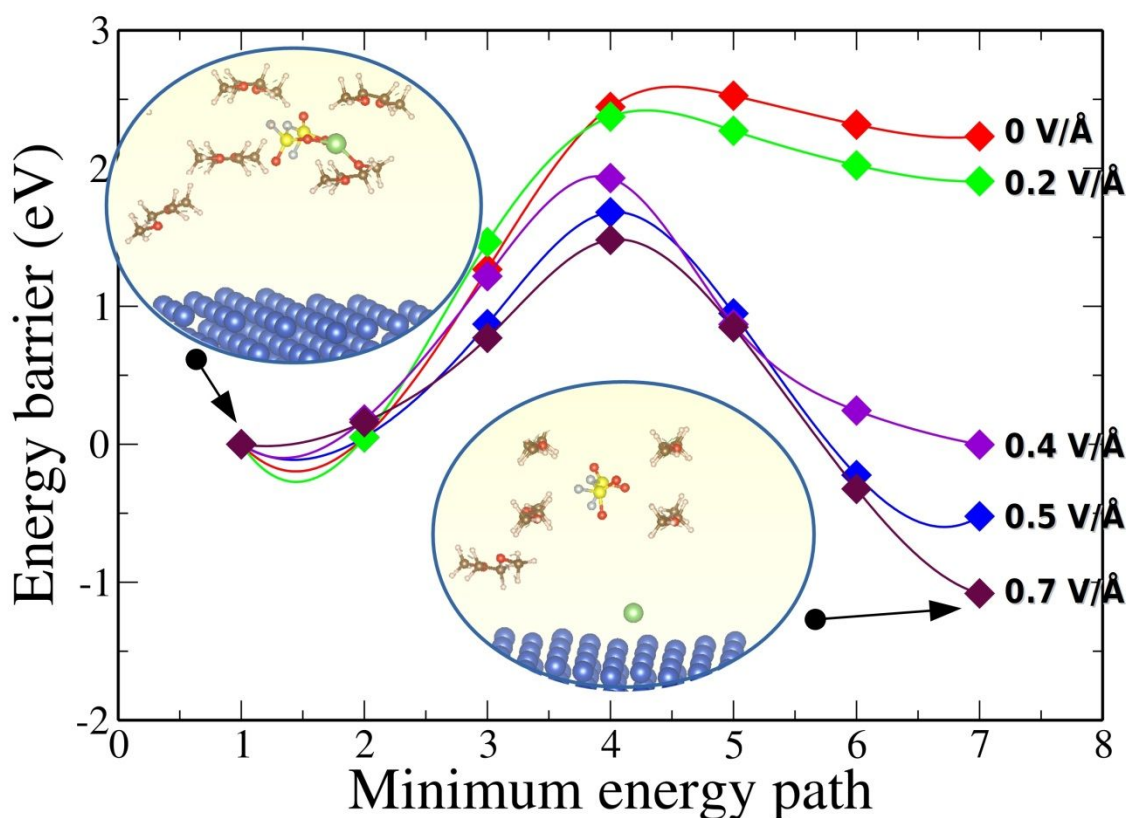
Figure 2. Electric field dependence of the kinetic energy profile of Li adsorption on Cu(001). Both substrate and molecules are placed between two electrodes (not shown), within the ESM QE

framework. Note that the energy barrier (difference between transition state and initial state) decreases significantly and the adsorption energy (difference between final and initial states) becomes endothermic as the electric field strength increases. The color code is the same as for Figure 1.

The picture shows the kinetic energy barrier of this two-step mechanism leading to the Li^+ deposition on the Cu(001) surface. One can see that an adsorption energy of 2.23 eV and an energy barrier of 2.52 eV in the absence of electric field, become -0.01 eV and 1.92 eV, respectively, for an electric field of 0.4 V/Å, *i.e.*, the cation deposition reaction becomes thermodynamically exothermic, although there still is a moderately high kinetic energy barrier. Larger electric fields result in more exothermic reaction energies. A field of 0.7 V/Å, which represents approximately an upper limit of the field strength for the supercell used in this work (beyond which electron leakage would occur at the supercell edges) produces a reaction energy for Li^+ adsorption of -1.08 eV and is the most kinetically favorable process.

In spite of the polarization orbitals formed as a consequence of the applied electric field, the Li^+ cation is not completely reduced (see the 1*s* PDOS in Figure 1b). This is anticipated, since Cu is a noble metal. A different substrate with larger degree of surface polarization should be used, if one expects to reduce Li ions already at the early stage of deposition. As additional information, Figures S2 and S3 of the Supporting Information show the change in the Fermi level and the height over the surface with the field strength for a Li^+ cation adsorbed on the Cu(001) surface. Larger, positive electric fields result in Fermi level shifts to higher energies, thus increasing the degree of reduction of the cation. Also, larger fields decrease the average height over the surface, due to the increase in the Coulombic attraction aforementioned.

This last statement takes us to an important point. If, instead of Li, a multivalent cation is considered, for instance $MgFSI^+$ (in order to allow a direct comparison between the

same states of charge), the results would be substantially different. The reason, naturally, is the distinct nature of both the vacant valence orbitals (now Mg^{2+}) and the polarization orbitals formed under the effect of the applied electric field. To confirm that, we performed additional calculations for DME-solvated $MgFSI^+$ on the Cu(001) surface. The results can be seen in the Supporting Information (Figure S4). Briefly, in absence of an electric field, the Mg^{2+} cation forms a tetravalent coordination with the surrounding oxygen ions (both from the FSI anion and the DME solvent) due to the double valence hole. The reaction energy to transform such structure into a trivalent coordinated system (similar to that of the LiFSI) is 0.45 eV, that is, it is an endothermic reaction (Figure S2-a). However, contrary to the LiFSI, the de-solvated $MgFSI^+$ molecule shows an exothermic adsorption energy on the Cu(001) surface, -0.86 eV. The reason can be easily understood on the basis of the electronic transfer from the $3s^2$ valence orbital aforementioned. Indeed, as can be seen on the Figure S4 of the Supporting Information, after adsorption on the surface the Mg^{2+} cation is no longer oxygen-tetravalent coordinated. Instead, the molecule undergoes a strong reorganization to form, besides the Mg^{2+}-O, a new Mg^{2+}-F^- bond. This increases the polarity of the Mg^{2+}-surface interaction, thus decreasing the adsorption energy. If the FSI anion is not present, the Mg^{2+} cation shows an endothermic adsorption energy, like Li^+ (last image in Figure S4-a). If the system is located between two electrodes and in the presence of an external electric field, the energetic effects are similar to those shown in Figure 2, just more pronounced. For example the adsorption energies of the de-solvated $MgFSI^+$ molecule become strongly exothermic and increasing field strength the deposition of naked cation becomes exothermic much faster than the case of Li. Indeed, Figure S4 shows that an electric field of only 0.2 V/Å suffices to exothermically deposit the Mg^{2+} cation.

b) *AIMD simulations of the deposition mechanism*. The greatest challenge addressed in this study was to discover whether it is possible to obtain a global picture of the whole cation deposition process by means of AIMD simulations, in order to unravel the

dynamic mechanism of cation deposition. Although the supercell used in this study is of moderate size, ESM QE simulations with an external electric field are both computationally demanding and difficult to converge. In order to speed up the calculations, for AIMD calculations we used a less dense k-mesh of 2x2x1 k-points, but no further constraints were imposed to the system. The external electric field was taken as 0.5 V/Å, in order to allow an exothermic adsorption reaction of the Li$^+$ cation. Some snapshots of the AIMD simulations are shown in Figure 3, whereas the Supporting Information (Figure S5) contains a much more complete set of intermediate states.

| 0.5 ps | 2 ps | 4 ps |
| 5.2 ps | 7.5 ps | 10.2 ps |

E=0.5 V/Å
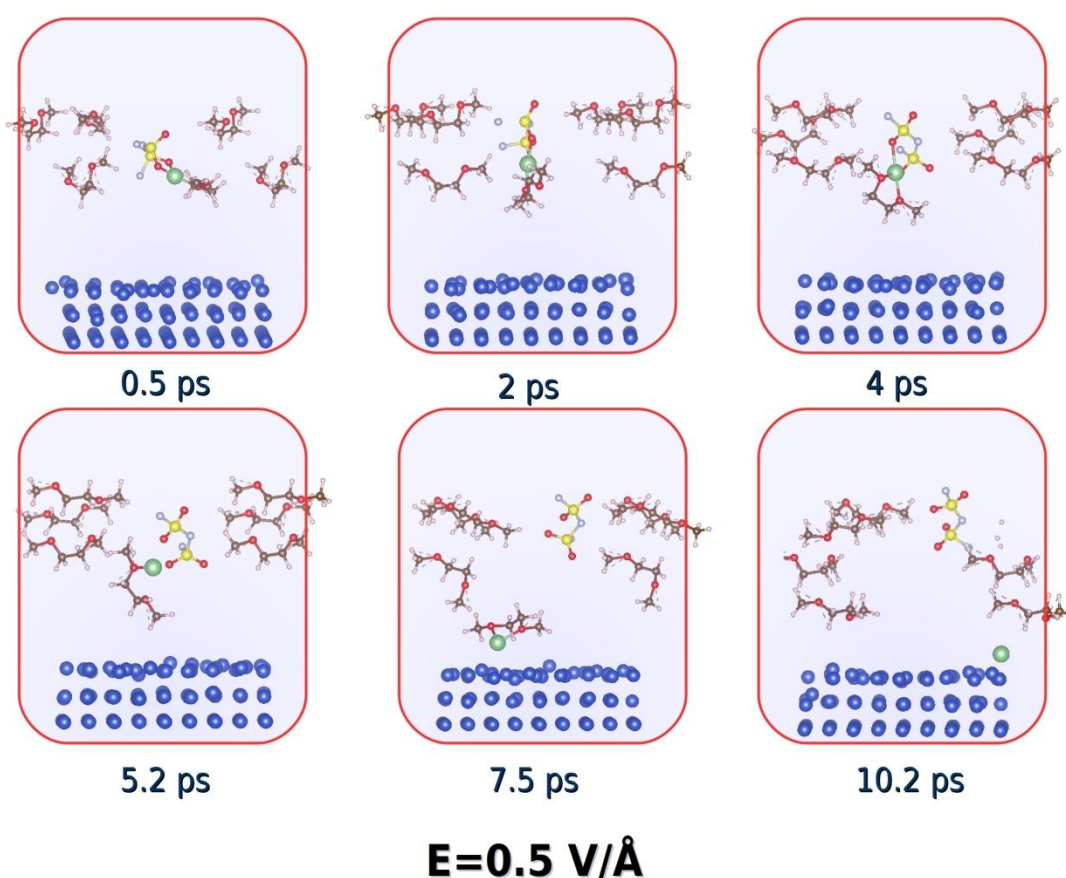
Figure 3. AIMD snapshots of DME-solvated LiFSI adsorption on Cu(001). Substrate and molecules are embedded between two electrodes within the ESM QE framework (not shown), between which there is an applied electric field of 0.5 V/Å. The successive images illustrate formation of the LiFSI/DME complex, and its reorientation under the electric field, followed by anion detachment and DME/Li$^+$ deposition. The color code is the same as for Figure 1.

The simulations were performed at 300 K. The results are extremely interesting, with the deposition process proceeding as follows. After only 0.5 ps, the Li^+ cation is already coordinated by three oxygen atoms (3O), as described previously. The overall shape of such 3O coordination sphere remains more or less symmetric during 2-3 ps, but the dipole moment formed due to the negatively charged FSI^- unit rotates the newly formed LiFSI-DME composite towards the surface (Figure 3). Then, after 4 ps, the number of oxygen atoms coordinating the Li^+ ion increases to four (4O), forming relatively long chemical bonds (2.1-2.3 Å), in an octahedron-like configuration. At 300 K and, assuming similar entropies, the enthalpy of the 4O-structure is slightly lower than that of the 3O-structure, ~0.12 eV, and such configuration remains as the most stable until 5 ps, approximately. Then, the proximity of the polarized Cu(001) surface strongly attracts one of the ending CH_3 units of the DME part of the composite, producing a stretching of three of the Li-O bonds. Then, the composite dissociates, forming a new DME-Li^+ compound. Once this compound is formed, the FSI^- anion becomes relatively volatile, leading to a rapid adsorption of the DME-Li^+ onto the polarized Cu(001) surface after 7.5 ps (Figure 3). After Li^+/DME deposition, the Coulombic attraction between the substrate and the DME weakens, which finally results in further complex dissociation and Li^+ deposition. However, in our simulations the DME molecule never completely desorbs from the Cu(001) surface, producing a pendulum effect that successively dissociates and recreates the DME-Li^+ composite. The presence of other anions might mitigate such effect, producing a "clean" Li growth on the metallic substrate. Thus, this may be one of the benefits of the high-concentrated electrolytes. In the Supporting Information (Figure S6), we show the average potential energy evolution during the AIMD simulations. This reflects the charge distribution changes during the deposition time. As can be seen in the figure, the initially electrolyte-localized electronic charge becomes almost a continuum after 10 ps. This facilitates the Li^+ adsorption onto the Cu(001) surface, but

considerably hinders the desorption of the DME solvent molecule bound to the Li^+ cation. Therefore, the use of low solvent densities (or, equivalently, high salt concentrations) becomes crucial to avoid the growth of non-uniform Li layers.

Effect of the applied bias (μ) on Li deposition on Cu(001). By using OBC as implemented in ESM QE, one can also study a slab in an electrochemical cell, modeled by a system placed between an electrode (with $\varepsilon_r=\infty$) and the vacuum ($\varepsilon_r=1$), which is appropriate to study systems under an applied bias, *i.e.*, to perform calculations under constant potential μ. The study of charged electrochemical interfaces represents both a challenge and a step forward for theoretical calculations, as obviously all the experiments occur under a specific applied bias [24]. Such applied bias, μ, is accounted for by means of obtaining the grand canonical potential as a function of the external potential μ, which then sets the Fermi energy to the targeted potential, thus including an extra degree of freedom in the Hamiltonian [46]. As said before, there has been a growing interest in the scientific community to simulating electrified interfaces, that is, electrochemical double layers, because of their relevance to energy conversion and storage devices. As such, by setting the electrode potential and letting the number of electrons equilibrate, one can easily obtain the charge vs potential curve, of which the average slope would correspond to the capacitance and the first derivative to the differential capacitance (DC). As an example, Figure 4 shows the capacitance and DC plots as a function of the applied potential for two cation systems: DME-solvated LiFSI and multivalent $MgFSI^+$ on Cu(001). The raw data is included in Table S3.

The average slopes correspond to a capacitance roughly of 0.26 $\mu F/cm^2$ for LiFSI and 0.37 $\mu F/cm^2$ for $MgFSI^+$. As it is already well-known, capacitance is the ability of a body to store an electrical charge. Even though the upper electrode is the result of the ESM QE implementation, Figure 4 provides an approximate way to graphically examining the

ease with which such applied voltages produce an effective result in our salt/solvent systems. As expected, salts containing multivalent cations such as Mg would display larger capacitance, especially for positive bias (less negative Fermi level), than Li-containing salts. Obviously, the difference lowers for negative bias, until the capacitance difference becomes practically indistinguishable.
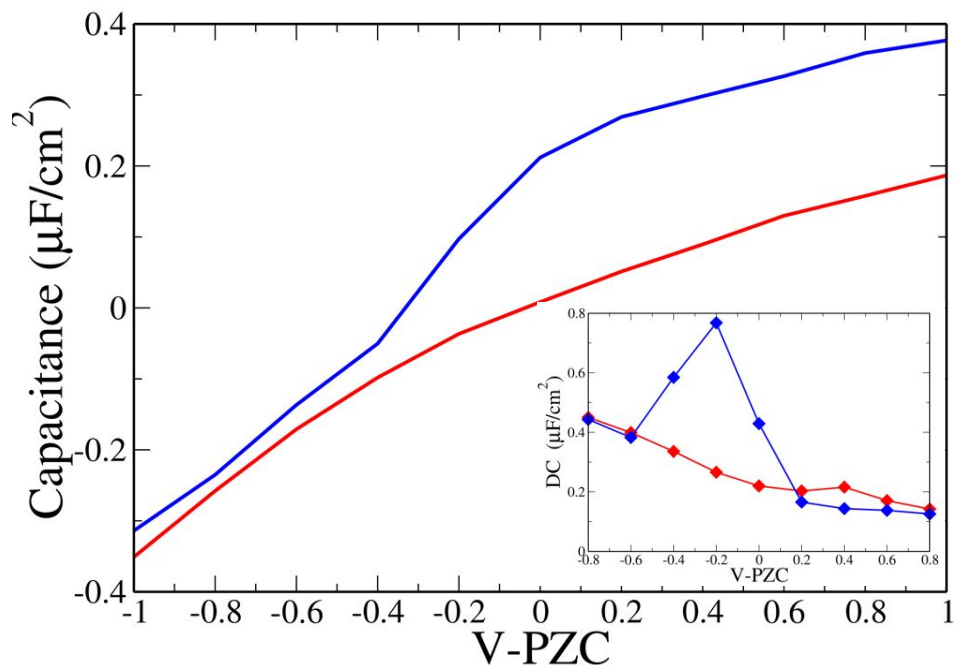
Figure 4. Capacitance *vs* applied potential (difference with the potential of zero charge, PZC) for DME-solvated LiFSI (red curve) and MgFSI[+] (blue curve) in an electrochemical double layer. One of the layers is the Cu(001) surface and the other is the "fictitious" electrode resulting from the ESM QE framework. The inset shows the differential capacitance.

For the sake of comparison, a capacitance of ~1.5 µF has been obtained for graphene oxide capacitors [51]. Also, the DC of the Mg salt shows a camel-shape form around -0.2 V, which is typical of systems with a high degree of oxidation. The DC of LiFSI displays a hardly perceptible bell-shape form around 0.4 V, characteristic of systems with a lower oxidation degree.

The dynamics of four salt/solvent combinations was investigated in this work: DME-solvated LiTFSI for two solvent concentrations (high- and low-density solvent; equivalent to low- and high salt concentration), DOL-solvated LiTFSI and DME-solvated LiNO$_3$. Thus, information relative to the effect of the applied bias on Li$^+$ deposition as a function of the solvent, solvent (salt) concentration and Li-containing salt structure was obtained.

As described in the Methodology section, we used an algorithm to take advantage of the combined strengths of ESM QE and VASP, in order to speed up the initial stages of cation deposition. The following discussion refers only to the final ESM QE calculations, that is, simulations with a true applied bias, except when explicitly noted.

a) *Cation deposition at low potentials: 0.2≤μ≤0.4 V*. The applied bias polarizes the metallic surface as well, similar to having an electric field between two electrodes, but now the driving force for molecular deposition on Cu(001) is slightly different. As the number of electrons in the system represents an additional variable to minimize during the calculations, solvent molecules with a more symmetric charge density such as DOL are expected to exert less influence on the dynamic evolution of the Li-containing molecular salt. Our results confirm such premise. In Figures 5 and 6, we show the final snapshots of the dynamic evolution of DME-solvated LiTFSI at high and low solvent (low- and high salt) concentrations, DOL-solvated LiTFSI and DME-solvated LiNO$_3$, respectively. As observed for LiFSI, the dominant configuration for DME-solvated LiTFSI involves the formation of an additional Li-oxygen bond, thus creating a LiTFSI-DME composite (Figure 5). At high solvent density, a 3O configuration is found where a 4O is observed at low solvent density (high salt concentration). The same consideration applies to LiNO$_3$-DME, where the large dipole moment of the LiNO$_3$ molecule quickly prompts the formation of a trivalent coordinated structure for the Li$^+$ cation. As expected, our AIMD simulations show practically no interaction between the LiTFSI and the DOL solvent molecules, thus resulting in a quick adsorption of the Li salt molecule on the polarized Cu(001) surface (after only 2.8 ps, according to our VASP results, for an

excess charge $\Delta\rho$=0.22e$^-$). Another remarkable difference is produced regarding the different solvent concentrations for DME-solvated LiTFSI. Indeed, low solvent concentration (or, equivalently, higher salt concentration) and low bias (0.2 V) result in the adsorption of the LiTFSI-DME composite after ~3 ps, by forming a surface-oxygen bond. The most stable configuration (Figure 5, top right) displays the DME perpendicular to the surface. The reason is that, similar to the previous section, the Coulombic attraction between the surface polarized vacant orbitals and one of the non-bound oxygen ions is much stronger than the interaction with the tetravalent coordinated Li$^+$ cation. In contrast, at high solvent concentration, the complex remains stable above the surface for longer times. This could be due to additional DME-driven interactions (for example H..F) stabilizing the complex.

0.2 V
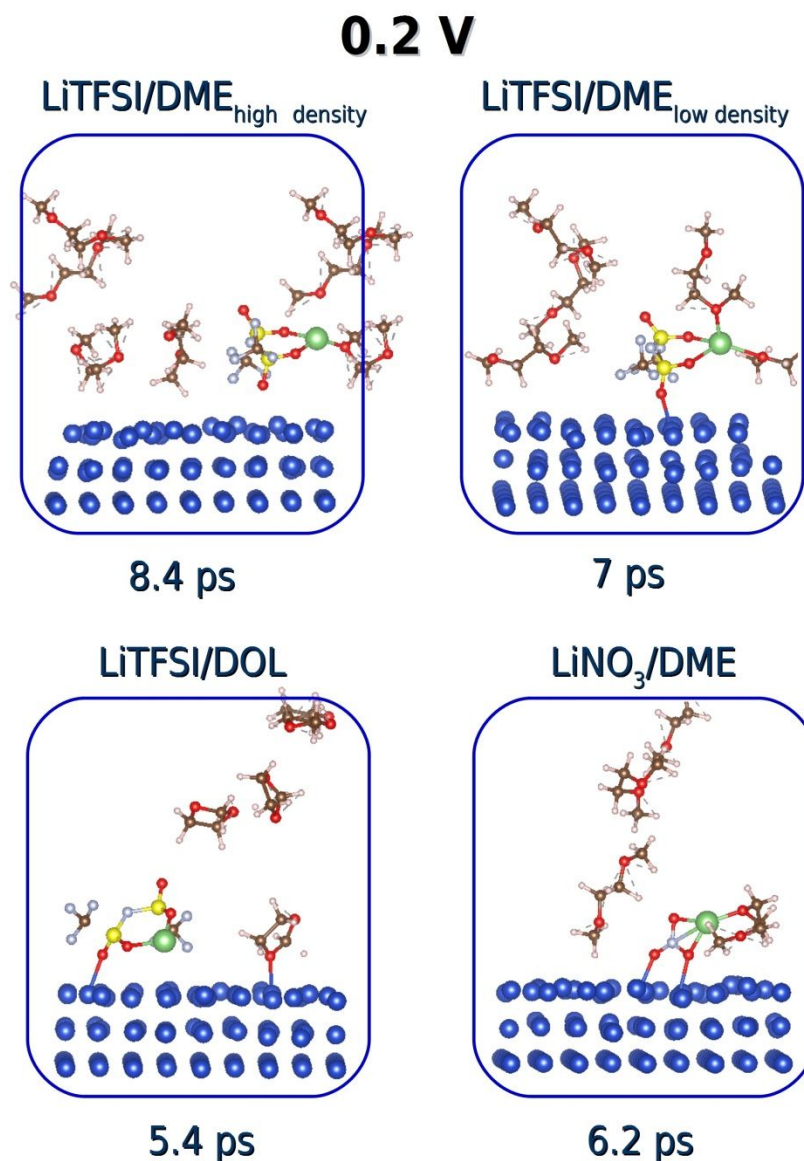
Figure 5. Final structures of the AIMD simulations of cation deposition on Cu(001), for two different salts, LiTFSI and LiNO$_3$, and solvents, DME and DOL, the first one at two different solvent (salt) concentrations. The system is placed in an electrochemical cell within the ESM QE framework, that is, an electrode in the upper part (not shown) and the vacuum beneath the surface, with an applied voltage of 0.2 V. Color code: Cu, blue; Li, green, O, red; C, brown, H, white; S, yellow; F, light purple; and N, light blue balls.

Low solvent concentration and moderate bias (0.4 V, Figure 6, bottom) lead to rapid adsorption of the Li salt without interaction with the solvent, after ~1.8 ps. High solvent

concentration and moderate bias (0.4 V, Figure 6, top) lead to the formation of tetra-coordinated LiTFSI-DME composite structure, where the DME is bent out of its original linear shape, forming a planar-octahedron-like Li-O structure.
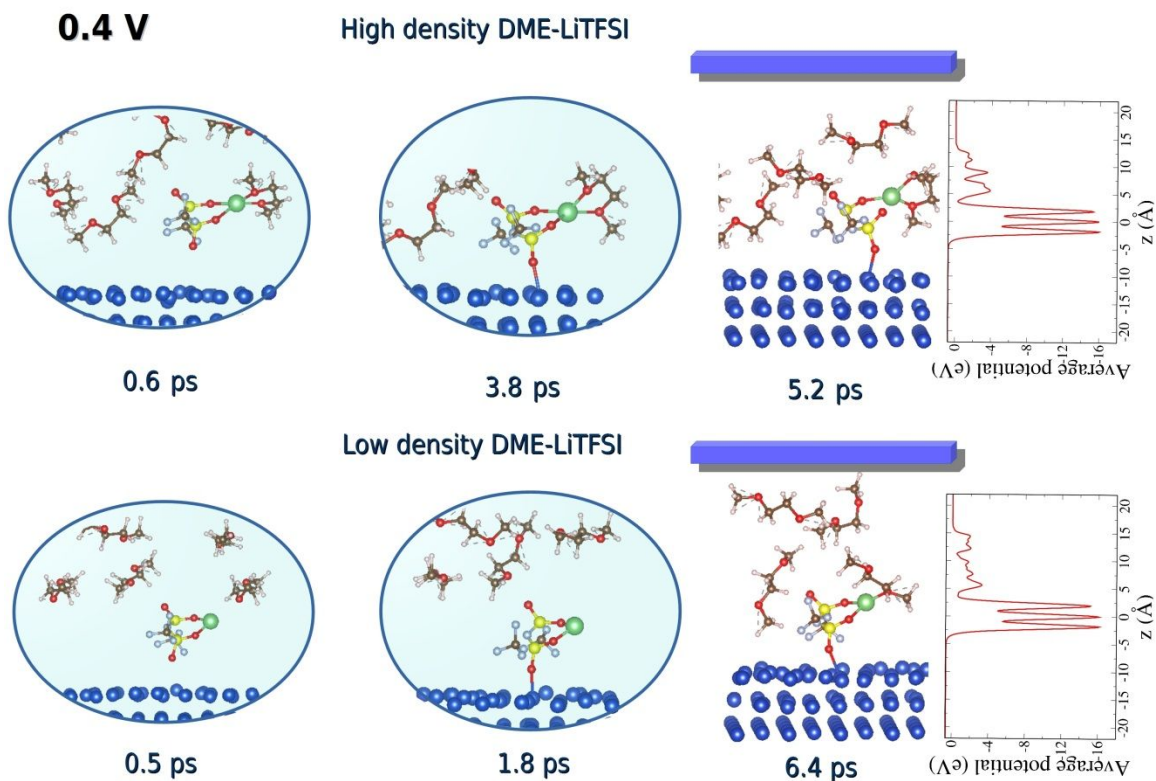
Figure 6. AIMD evolution of cation deposition from DME-solvated LiTFSI on Cu(001), for two different solvent concentrations under an applied voltage of 0.4 V. The system is placed in an electrochemical cell within the ESM QE framework, that is, an electrode in the upper part and the vacuum beneath the surface. In both cases the final configuration is similar; however the evolution is different. At high solvent (low salt) concentration there is a slow deposition of the complex salt/solvent, whereas in the low solvent (high salt) case, the naked salt deposits first but it is followed by solvent complexation. The average potential energies (Hartree and local) for the final configurations are shown in the right-hand side, showing a highly localized electrolyte profile at the high solvent concentration compared with the more distributed profile in the low solvent condition. The color code is the same as for Figure 4.

The deposition dynamics of the complex structure at high solvent concentration is slower than the one at low solvent (high salt) concentration, needing about ~4 ps to get adsorbed on the substrate. The structure of the adsorbed LiTFSI, originally solvated in DOL (Figure 5, at low bias), is similar to the one obtained at low DME solvent concentration and moderate bias. Yet the Li^+ cation is only partially reduced, in spite of the interaction with the surface polarization orbitals (q_{Li}=0.42e$^-$). On the other hand, the $LiNO_3$-DME composite is rapidly adsorbed on the Cu(001) surface, forming two strong surface-oxygen bonds (Figure 5, low bias), with the DME solvent molecule parallel to the surface, in order to maximize the Li-O interaction strength. Interestingly, as discussed above, for low DME concentration and low bias, after ~5 ps a LiTFSI-(DME)$_2$ composite is formed at the Cu(001) surface, with the Li^+ cation adopting a non-planar, tetrahedral configuration (Figure 5, top right). On the other hand, a LiTFSI-DME composite is formed for moderate bias (0.4 V) after the same AIMD simulation time (Figure 6, bottom). Finally, after t>6 ps, only two of the systems are found relatively close to the ultimate goal, that is, Li deposition. i) For high DME concentration and moderate bias, the two Li-TFSI bonds of the planar-octahedron like Li-O structure stretched almost to the rupture point (not shown), leaving a DME-Li composite similar to the structure seen in Figure 3. Thus, we might expect anion reduction and Li^+/DME deposition. ii) For the previously DOL solvated (Figure 5), adsorbed LiTFSI loses the organic tail, two (CF_3) groups, with the remaining TFSI fragment adopting an overall-linear shape parallel to the Cu(001) surface, which leads to Li adsorption. At this point, the Li^+ cation is more than halfway reduced, with a total charge of q(Li)=0.62e$^-$.

b) *Cation deposition at high potentials: 0.6≤μ≤0.8 V*. The most remarkable difference of the AIMD simulations of cation deposition at high potentials lies in the fact that, although the overall molecular structures and deposition mechanisms are relatively similar to

those obtained at lower potentials, the reaction times are much faster, as we will quantify at the end of this section. This may result in the acceleration of cation deposition or in the formation of undesired intermediate species. Then, although not always trivial, choosing an appropriate voltage window seems to be key to ensure the final attainment of the desired reaction product. A summary of the obtained results is depicted in Figures 7 and 8. For instance, for DME-solvated LiTFSI, the adsorption of a LiTFSI-DME composite is rapidly seen, after only ~1 ps and for low and high solvent densities (Figure 7 a and b). The Li^+ cation always forms an overall trigonal shape with the surrounding oxygen ions. Then, after ~2.5 ps, the overall shape of the LiTFSI molecule changes considerably, tilting over the surface, which for larger bias, even leads to the interaction of the surface Cu atoms with some of the negatively charged atomic sites, like F. However, Li^+ cations remain in their trigonal oxygen coordination. Major changes can be noted after 3 ps. Especially for μ=0.6 V, a $LiTFSI-(DME)_2$ composite is formed, which applies a tensile strain on the Li-TFSI oxygen bonds, producing a less symmetric and more distorted molecular geometry (Figure 7a).
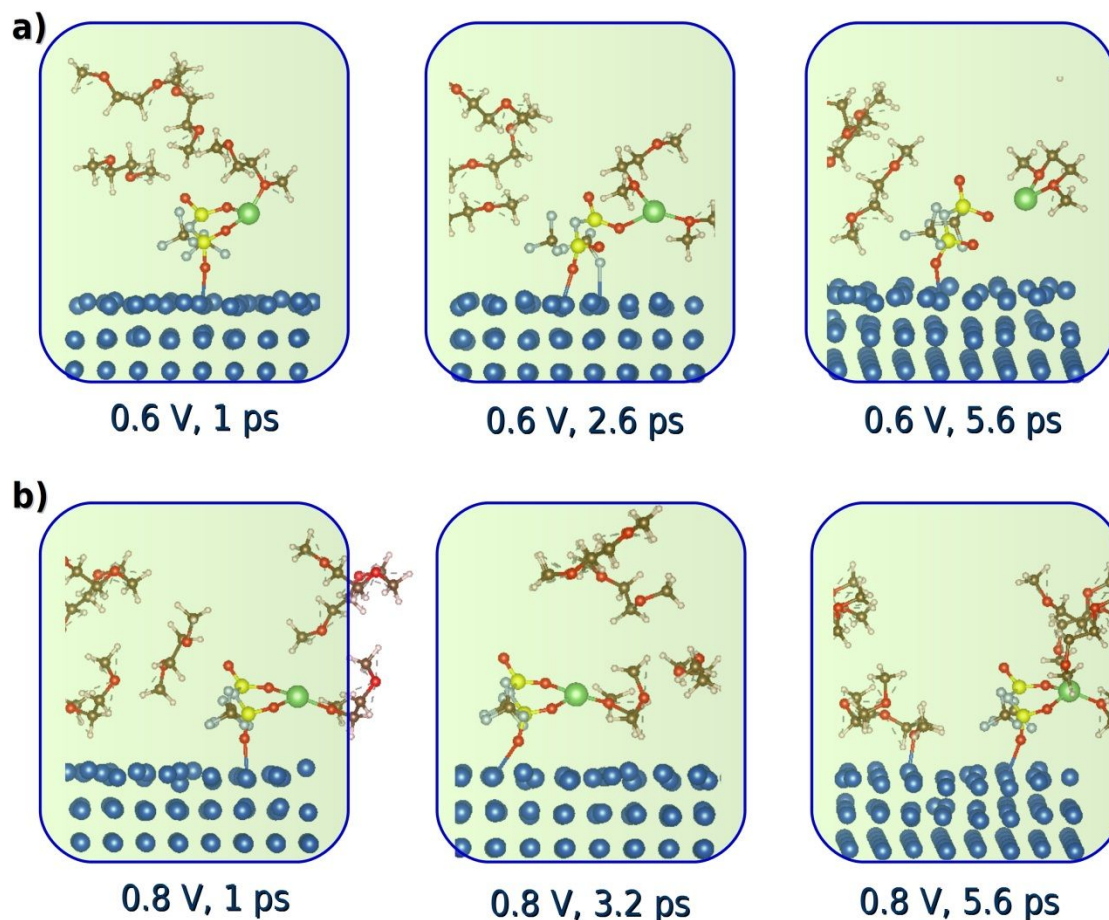
Figure 7. AIMD evolution of cation deposition from DME-solvated LiTFSI on Cu(001), for two different solvent concentrations: a) low density, and b) high density, under an applied voltage of 0.6 and 0.8 V, respectively. Substrate and adsorbates are placed in an electrochemical cell within the ESM QE framework, that is, an electrode in the upper part (not shown) and the vacuum beneath the surface. The color code is the same as for Figure 4.

Interestingly, the Li$^+$ cation retains the triple oxygen coordination, as only one of the oxygen bonds with the anion is broken, and a new LiO bond is formed with a new DME molecule. After 5 ps and for the low solvent concentration, the Li-TFSI bond is broken and a new Li-DME composite is formed (Figure 7a). Whereas for the high density solvent the process requires more time, because of the "availability" of DME molecules to form new LiTFSI-DME composites. Figure 7b illustrates such process starting by an

adsorbed LiTFSI/DME composite, connected to the surface via O-Cu bonds. At longer times, solvent molecules become also adsorbed on the surface.

Figure 8 a and b illustrate the effect of high potential bias (0.6 and 0.8 V) for the cases of LiTFSI in DOL-based solution, and LiNO3 in DME solution. The surface adsorption of a $LiNO_3$-DME composite (Figure 8b) is also produced swiftly at high potentials, and the most stable configuration now includes a $LiNO_3$ structure perpendicular to the Cu(001) surface (at t~3 ps), where only one surface-oxygen bond is formed (in contrast to that at lower potential, shown in Figure 5).

a)

0.6 V, 0.4 ps   0.6 V, 2.2 ps   0.6 V, 3.6 ps

b)

0.8 V, 1.8 ps   0.8 V, 3.0 ps   0.8 V, 4.8 ps
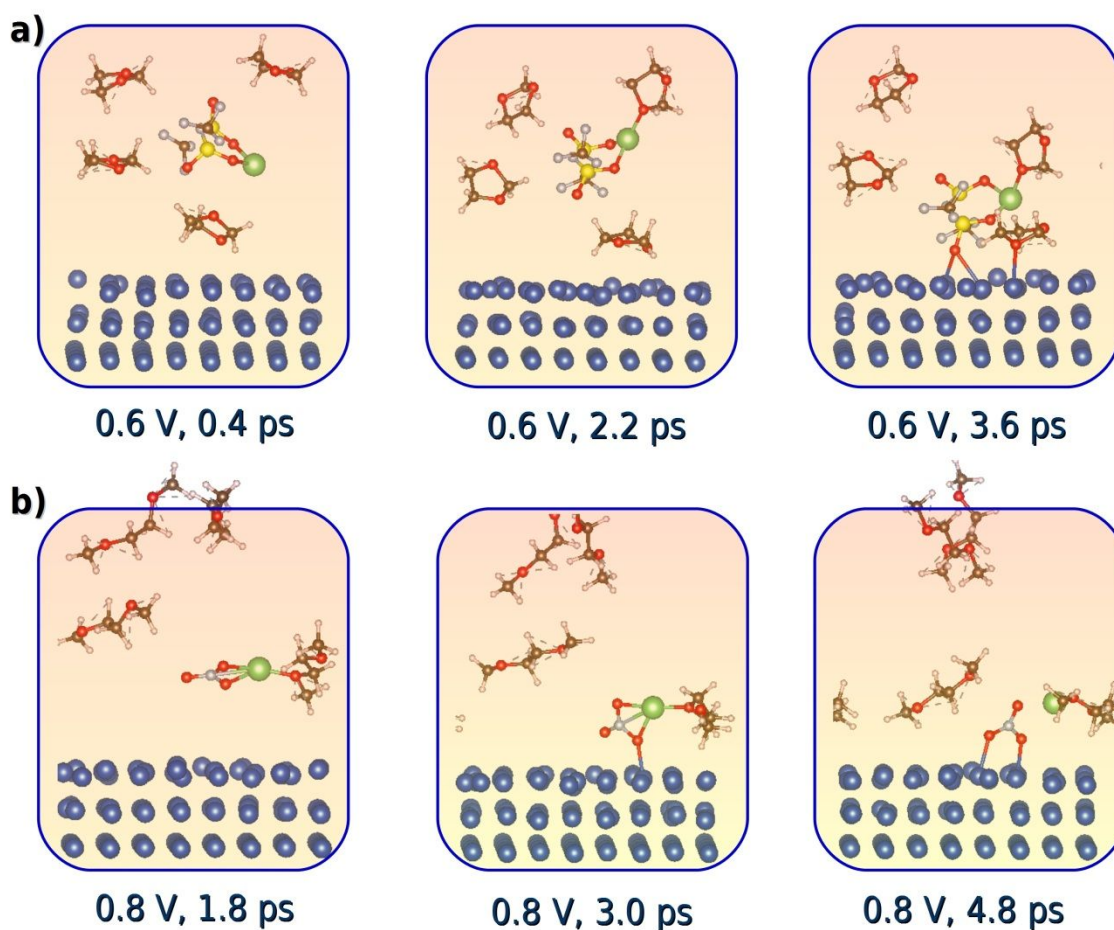
Figure 8. AIMD evolution of cation deposition from: a) DOL-solvated LiTFSI, and b) DME-solvated $LiNO_3$ on Cu(001), under an applied voltage of 0.6 and 0.8 V, respectively. Substrate and adsorbates are placed in an electrochemical cell within the ESM QE framework, that is, an

electrode in the upper part (not shown) and the vacuum beneath the surface. The color code is the same as for Figure 4.

However, after 4 ps, the Li^+ cation is dissociated from the NO_3 main body, and a new Li-DME composite is formed. The adsorption of the NO_3 anion is possibly the starting point of the anion decomposition. On the contrary, as mentioned earlier, the highly symmetric charge density of the DOL solvent molecule leads to a rapid deposition of one of such molecules (after only ~0.5 ps, see Figure 8a) for an applied voltage of 0.6 V. Then, another LiTFSI-DOL composite is formed, with the Li^+ ion forming a triangular bond with the surrounding oxygen atoms. Finally, after only 3.6 ps, such composite is adsorbed onto the Cu surface. The most stable adsorbed structure (Figure 8a) displays an oxygen ion adsorbed on a surface hollow site, whereas the Li^+ ion now forms a trigonal prism configuration with one of the oxygen atoms of the DOL molecule, which is perpendicular to the plane formed by the cation and the oxygen atoms of the TFSI unit it is bound to.

All these results describe summarily the cation deposition process as a function of the composition and the applied bias. Our results suffice to state that if the goal were obtaining a smooth metal deposition, the voltage window and the nature of the electrolyte must be properly chosen in order to avoid the deposition of undesired reaction products for a specific solvent concentration.

Most of the reactions showed in this work seem to indicate that at the very initial stages of electrolyte/electrode dynamics under an applied field, composites of the form Li-DME are the main deposition product on Cu surfaces. As was shown earlier in this section, medium-strength electric fields and simulation times (but longer than those shown here) suffice to break such bond, which will facilitate further deposition of Li ions. Therefore, to avoid organic contamination during Li deposition, not only the voltage window but the deposition times must be properly taken into account.

Finally, we would like to say that high potentials result in much faster deposition times, something that is not always desirable. As such, cation deposition becomes an equilibrium process between ion adsorption and desorption of the undesired intermediate reaction species. In order to quantify such time differences, we resort to a simple Langmuir isotherm model and the Arrhenius equation to obtain cation adsorption coverages. The methodology was used in our previous publication [52] and is described in the Supporting Information, using also basic circuit theory modeling to correlate the applied bias with the sticking coefficient for adsorption on the Cu(001) surface. As can be seen in Figure S7, saturation coverage is rapidly achieved at high potential regimes, whereas for lower potentials much more time (partial pressure, which for electrolyte solutions may be equivalent to molecular concentrations and could be proportional to current rates) is needed in order to successfully deposit a monolayer of cations on the Cu(001) surface.

Conclusions

In this work, we explored the factors determining the mechanisms of cation deposition on a metallic surface, from different salt/solvent mixtures. We found that there is a practical limit for the solvent concentration around each Li^+ ion-containing salt molecule, and that such limit is given by the cation-oxygen polyhedral structure. Cation reduction at the Cu(001) surface is an insufficient condition for Li growth, given the endothermic nature of such deposition reaction. Moreover, such cation deposition process is a two-step mechanism. The first step is driven by kinetics, whereas the second step involves the dissociation of the cation-containing salt. In the presence of an external electric field, surface polarization orbitals increase the cation-metal Coulombic interaction, leading to an overall exothermic deposition process. However, reductive stability of the cation is not completely achieved, due to the noble character of the Cu(001) surface. This can be

altered with the use of multivalent cations, as demonstrated for $(MgFSI)^+$. AIMD simulations show that the formation of an intermediate $DME-Li^+$ composite is the key to Li deposition, with the use of low-solvent densities (high salt concentration) becoming crucial to allow the growth of uniform Li layers.

When the system was designed like an electrochemical cell, it was found that externally applied bias determines the cation deposition mechanisms to a very large extent. By considering different salt/solvent combinations and two sets of potential regimes, we found that solvent structures with symmetric charge density, such as DOL, exert less influence on cation deposition, whereas salts with a large electric dipole moment, such as $LiNO_3$, quickly prompt the formation of salt-solvent intermediate composites. For a low potential regime, low solvent (high salt) concentrations also result in fast salt adsorption with no solvent interaction. Such adsorbed structures always entail the formation of a surface-oxygen bond, as well as different Li^+-O polyhedra, depending on the salt/solvent pair. Finally, a high potential regime always results in accelerated deposition reactions, leading to the adsorption of salt-solvent composites, even when using DOL as solvent. Thus, the use of moderate voltage windows and rapid deposition times (for instance, by controlling the driving force given by electrolyte concentration and/or current rate) seems to represent the optimal choice for cation deposition and uniform growth of metal anode layers, in order to achieve stable electrode-electrolyte interfaces.

Acknowledgments

References

(1)   Tarascon, J. M.; Armand, M. Issues and challenges facing rechargeable lithium batteries. *Nature* **2001**, *414*, 359-367.

(2)   Manthiram, A.; Knight, J. C.; Myung, S. T.; Oh, S. M.; Sun, Y. K. Nickel-Rich and Lithium-Rich Layered Oxide Cathodes: Progress and Perspectives. *Adv. Energy Mater.* **2016**, *6*, 23.

(3)   Crabtree, G.; Kocs, E.; Trahey, L. The energy-storage frontier: Lithium-ion batteries and beyond. *Mrs Bulletin* **2015**, *40*, 1067-1078.

(4)   Nitta, N.; Wu, F. X.; Lee, J. T.; Yushin, G. Li-ion battery materials: present and future. *Mater. Today* **2015**, *18*, 252-264.

(5)   Luntz, A. C.; Voss, J.; Reuter, K. Interfacial Challenges in Solid-State Li Ion Batteries. *J. Phys. Chem. Lett.* **2015**, *6*, 4599-4604.

(6)   Nykvist, B.; Nilsson, M. Rapidly falling costs of battery packs for electric vehicles. *Nat. Clim. Chang.* **2015**, *5*, 329-332.

(7)   Yang, Z. G.; Zhang, J. L.; Kintner-Meyer, M. C. W.; Lu, X. C.; Choi, D. W.; Lemmon, J. P.; Liu, J. Electrochemical Energy Storage for Green Grid. *Chem. Rev.* **2011**, *111*, 3577-3613.

(8)   Goodenough, J. B. Electrochemical energy storage in a sustainable modern society. *Energy Environ. Sci.* **2014**, *7*, 14-18.

(9)   Gauthier, M.; Carney, T. J.; Grimaud, A.; Giordano, L.; Pour, N.; Chang, H. H.; Fenning, D. P.; Lux, S. F.; Paschos, O.; Bauer, C.; Magia, F.; Lupart, S.; Lamp, P.; Shao-Horn, Y. Electrode-Electrolyte Interface in Li-Ion Batteries: Current Understanding and New Insights. *J. Phys. Chem. Lett.* **2015**, *6*, 4653-4672.

(10)   Xu, K. Electrolytes and Interphases in Li-Ion Batteries and Beyond. *Chem. Rev.* **2014**, *114*, 11503-11618.

(11)   Ming, J.; Cao, Z.; Wahyudi, W.; Li, M. L.; Kumar, P.; Wu, Y. Q.; Hwang, J. Y.; Hedhili, M. N.; Cavallo, L.; Sun, Y. K.; Li, L. J. New Insights on Graphite Anode Stability in Rechargeable Batteries: Li Ion Coordination Structures Prevail over Solid Electrolyte Interphases. *Acs Energy Letters* **2018**, *3*, 335-340.

(12)   Leung, K.; Soto, F. A.; Hankins, K.; Balbuena, P. B.; Harrison, K. L. Stability of Solid Electrolyte Interphase Components on Li metal and Reactive Anode Material Surfaces. *J. Phys. Chem. C* **2016**, *120*, 6302-6313.

(13)   Bruce, P. G.; Freunberger, S. A.; Hardwick, L. J.; Tarascon, J. M. Li-O-2 and Li-S batteries with high energy storage. *Nat. Mater.* **2012**, *11*, 19-29.

(14)   Li, J. C.; Ma, C.; Chi, M. F.; Liang, C. D.; Dudney, N. J. Solid Electrolyte: the Key for High-Voltage Lithium Batteries. *Adv. Energy Mater.* **2015**, *5*, 6.

(15)   Chen, S. R.; Zheng, J. M.; Mei, D. H.; Han, K. S.; Engelhard, M. H.; Zhao, W. G.; Xu, W.; Liu, J.; Zhang, J. G. High-Voltage Lithium-Metal Batteries Enabled by Localized High-Concentration Electrolytes. *Adv. Mater.* **2018**, *30*, 7.

(16)   Jiao, S. H.; Ren, X. D.; Cao, R. G.; Engelhard, M. H.; Liu, Y. Z.; Hu, D. H.; Mei, D. H.; Zheng, J. M.; Zhao, W. G.; Li, Q. Y.; Liu, N.; Adams, B. D.; Ma, C.; Liu,

J.; Zhang, J. G.; Xu, W. Stable cycling of high-voltage lithium metal batteries in ether electrolytes. *Nature Energy* **2018**, *3*, 739-746.

(17)   Ren, X. D.; Chen, S. R.; Lee, H.; Mei, D. H.; Engelhard, M. H.; Burton, S. D.; Zhao, W. G.; Zheng, J. M.; Li, Q. Y.; Ding, M. S.; Schroeder, M.; Alvarado, J.; Xu, K.; Meng, Y. S.; Liu, J.; Zhang, J. G.; Xu, W. Localized High-Concentration Sulfone Electrolytes for High-Efficiency Lithium-Metal Batteries. *Chem* **2018**, *4*, 1877-1892.

(18)   Yu, L.; Chen, S. R.; Lee, H.; Zhang, L. C.; Engelhard, M. H.; Li, Q. Y.; Jiao, S. H.; Liu, J.; Xu, W.; Zhang, J. G. A Localized High-Concentration Electrolyte with Optimized Solvents and Lithium Difluoro(oxalate)borate Additive for Stable Lithium Metal Batteries. *Acs Energy Letters* **2018**, *3*, 2059-2067.

(19)   Yang, C. P.; Zhang, L.; Liu, B. Y.; Xu, S. M.; Hamann, T.; McOwen, D.; Dai, J. Q.; Luo, W.; Gong, Y. H.; Wachsman, E. D.; Hu, L. B. Continuous plating/stripping behavior of solid-state lithium metal anode in a 3D ion-conductive framework. *Proc. Natl. Acad. Sci. U. S. A.* **2018**, *115*, 3770-3775.

(20)   Steinruck, H. G.; Cao, C. T.; Tsao, Y.; Takacs, C. J.; Konovalov, O.; Vatamanu, J.; Borodin, O.; Toney, M. F. The nanoscale structure of the electrolyte-metal oxide interface. *Energy Environ. Sci.* **2018**, *11*, 594-602.

(21)   Richards, W. D.; Miara, L. J.; Wang, Y.; Kim, J. C.; Ceder, G. Interface Stability in Solid-State Batteries. *Chem. Mat.* **2016**, *28*, 266-273.

(22)   Santosh, K. C.; Xiong, K.; Longo, R. C.; Cho, K. Interface phenomena between Li anode and lithium phosphate electrolyte for Li-ion battery. *J. Power Sources* **2013**, *244*, 136-142.

(23)   Stegmaier, S.; Voss, J.; Reuter, K.; Luntz, A. C. Li+ Defects in a Solid-State Li Ion Battery: Theoretical Insights with a Li3OCl Electrolyte. *Chem. Mat.* **2017**, *29*, 4330-4340.

(24)   Baskin, A.; Prendergast, D. Exploration of the Detailed Conditions for Reductive Stability of Mg(TFSI)(2) in Diglyme: Implications for Multivalent Electrolytes. *J. Phys. Chem. C* **2016**, *120*, 3583-3594.

(25)   Soto, F. A.; Ma, Y.; Martinez-DeLaHoz, J. M.; Seminario, J. M.; Balbuena, P. B. Formation and Growth Mechanisms of Solid-Electrolyte Interphase Layers in Rechargeable Batteries *Chem. Mater.* **2015**, *27*, 7990-8000.

(26)   Pei, A.; Zheng, G. Y.; Shi, F. F.; Li, Y. Z.; Cui, Y. Nanoscale Nucleation and Growth of Electrodeposited Lithium Metal. *Nano Lett.* **2017**, *17*, 1132-1139.

(27)   Camacho-Forero, L. E.; Smith, T. W.; Bertolini, S.; Balbuena, P. B. Reactivity at the Lithium-Metal Anode Surface of Lithium-Sulfur Batteries. *J. Phys. Chem. C* **2015**, *119*, 26828-26839.

(28)   Camacho-Forero, L. E.; Smith, T. W.; Balbuena, P. B. Effects of High and Low Salt Concentration in Electrolytes at Lithium-Metal Anode Surfaces. *J. Phys. Chem. C* **2017**, *121*, 182-194.

(29)   Horrocks, G. A.; Braham, E. J.; Liang, Y. F.; De Jesus, L. R.; Jude, J.; Velazquez, J. M.; Prendergast, D.; Banerjee, S. Vanadium K-Edge X-ray Absorption Spectroscopy as a Probe of the Heterogeneous Lithiation of V2O5: First-Principles Modeling and Principal Component Analysis. *J. Phys. Chem. C* **2016**, *120*, 23922-23932.

(30)   Giannozzi, P.; Andreussi, O.; Brumme, T.; Bunau, O.; Nardelli, M. B.; Calandra, M.; Car, R.; Cavazzoni, C.; Ceresoli, D.; Cococcioni, M.; Colonna, N.; Carnimeo, I.; Dal Corso, A.; de Gironcoli, S.; Delugas, P.; DiStasio, R. A.; Ferretti, A.; Floris, A.; Fratesi, G.; Fugallo, G.; Gebauer, R.; Gerstmann, U.; Giustino, F.; Gorni, T.; Jia, J.; Kawamura, M.; Ko, H. Y.; Kokalj, A.; Kucukbenli, E.; Lazzeri, M.; Marsili, M.;

Marzari, N.; Mauri, F.; Nguyen, N. L.; Nguyen, H. V.; Otero-de-la-Roza, A.; Paulatto, L.; Ponce, S.; Rocca, D.; Sabatini, R.; Santra, B.; Schlipf, M.; Seitsonen, A. P.; Smogunov, A.; Timrov, I.; Thonhauser, T.; Umari, P.; Vast, N.; Wu, X.; Baroni, S. Advanced capabilities for materials modelling with QUANTUM ESPRESSO. *J. Phys.-Condes. Matter* **2017**, *29*.

(31)   Giannozzi, P.; Baroni, S.; Bonini, N.; Calandra, M.; Car, R.; Cavazzoni, C.; Ceresoli, D.; Chiarotti, G. L.; Cococcioni, M.; Dabo, I.; Dal Corso, A.; de Gironcoli, S.; Fabris, S.; Fratesi, G.; Gebauer, R.; Gerstmann, U.; Gougoussis, C.; Kokalj, A.; Lazzeri, M.; Martin-Samos, L.; Marzari, N.; Mauri, F.; Mazzarello, R.; Paolini, S.; Pasquarello, A.; Paulatto, L.; Sbraccia, C.; Scandolo, S.; Sclauzero, G.; Seitsonen, A. P.; Smogunov, A.; Umari, P.; Wentzcovitch, R. M. QUANTUM ESPRESSO: a modular and open-source software project for quantum simulations of materials. *J. Phys.-Condes. Matter* **2009**, *21*.

(32)   Kresse, G.; Furthmuller, J. Efficiency of Ab-Initio Total Energy Calculations for Metals and Semiconductors using a Plane-Wave Basis Set. *Comp. Mat. Sci.* **1996**, *6*, 15-50.

(33)   Kresse, G.; Hafner, J. Ab initio molecular dynamics for open-shell transition metals. *Physical Review B: Condensed Matter and Materials Physics* **1993**, *48*, 13115-13118.

(34)   Bloechl, P. E. Projector augmented-wave method. *Physical Review B: Condensed Matter* **1994**, *50*, 17953-17979.

(35)   Kresse, G.; Joubert, D. From ultrasoft pseudopotentials to the projector augmented-wave method. *Phys. Rev. B* **1999**, *59*, 1758-1775.

(36)   Quantum Espresso web site. 2019).

(37)   Monkhorst, H. J.; Pack, J. D. Special points for Brillouin-zone integrations. *Phys. Rev. B* **1976**, *13*, 5188-5192.

(38)   Perdew, J. P.; Burke, K.; Ernzerhof, M. Generalized Gradient Approximation Made Simple. *Phys. Rev. Lett.* **1996**, *77*, 3865-3868.

(39)   Grimme, S.; Antony, J.; Ehrlich, S.; Krieg, H. A consistent and accurate ab initio parametrization of density functional dispersion correction (DFT-D) for the 94 elements H-Pu. *J. Chem. Phys.* **2010**, *132*.

(40)   Barone, V.; Casarin, M.; Forrer, D.; Pavone, M.; Sambi, M.; Vittadini, A. Role and Effective Treatment of Dispersive Forces in Materials: Polyethylene and Graphite Crystals as Test Cases. *J. Comput. Chem.* **2009**, *30*, 934-939.

(41)   Longo, R. C.; Cho, K.; Schmidt, W. G.; Chabal, Y. J.; Thissen, P. Monolayer Doping via Phosphonic Acid Grafting on Silicon: Microscopic Insight from Infrared Spectroscopy and Density Functional Theory Calculations. *Advanced Functional Materials* **2013**, *23*, 3471-3477.

(42)   Jonsson, H.; Mills, G.; Jacobsen, K. W.: *Classical and Quantum Dynamics in Condensed Phase Simulations*; World Scientific: Singapore, 1998.

(43)   Henkelman, G.; Jonsson, H. Improved tangent estimate in the nudged elastic band method for finding minimum energy paths and saddle points. *J. Chem. Phys.* **2000**, *113*, 9978-9985.

(44)   Henkelman, G.; Uberuaga, B. P.; Jonsson, H. A climbing image nudged elastic band method for finding saddle points and minimum energy paths. *J. Chem. Phys.* **2000**, *113*, 9901-9904.

(45)   Otani, M.; Sugino, O. First-principles calculations of charged surfaces and interfaces: A plane-wave nonrepeated slab approach. *Phys. Rev. B* **2006**, *73*, 11.

(46)   Bonnet, N.; Morishita, T.; Sugino, O.; Otani, M. First-Principles Molecular Dynamics at a Constant Electrode Potential. *Phys. Rev. Lett.* **2012**, *109*, 5.

(47)   Hamada, I.; Sugino, O.; Bonnet, N.; Otani, M. Improved modeling of electrified interfaces using the effective screening medium method. *Phys. Rev. B* **2013**, *88*, 4.

(48)   Kresse, G.; Furthmuller, J. Efficiency of ab-initio total energy calculations for metals and semiconductors using a plane-wave basis set. *Comput. Mater. Sci.* **1996**, *6*, 15-50.

(49)   Haruyama, J.; Ikeshoji, T.; Otani, M. Electrode potential from density functional theory calculations combined with implicit solvation theory. *Phys. Rev. Mater.* **2018**, *2*, 11.

(50)   Haruyama, J.; Ikeshoji, T.; Otani, M. Analysis of Lithium Insertion/Desorption Reaction at Interfaces between Graphite Electrodes and Electrolyte Solution Using Density Functional plus Implicit Solvation Theory. *J. Phys. Chem. C* **2018**, *122*, 9804-9810.

(51)   Neto, A. J. P.; Fileti, E. E. Differential Capacitance and Energetics of the Electrical Double Layer of Graphene Oxide Supercapacitors: Impact of the Oxidation Degree. *J. Phys. Chem. C* **2018**, *122*, 21824-21832.

(52)   Longo, R. C.; Addou, R.; Santosh, K. C.; Noh, J. Y.; Smyth, C. M.; Barrera, D.; Zhang, C. X.; Hsu, J. W. P.; Wallace, R. M.; Cho, K. Intrinsic air stability mechanisms of two-dimensional transition metal dichalcogenide surfaces: basal versus edge oxidation. *2d Materials* **2017**, *4*.

Journal of Materials Chemistry A

Table of Contents Figure
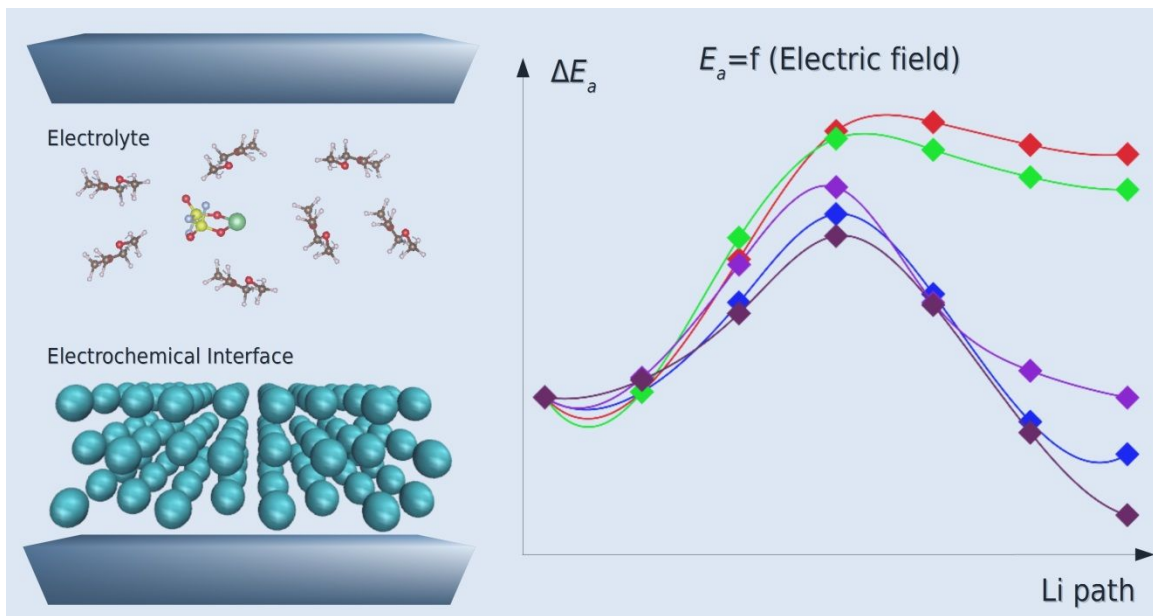
An applied potential modifies the reaction energy pathway favoring cation

electrodeposition at the electrochemical interface